ISBN: 978-3-95450-200-4 doi:10.18429/JACoW-ICAP2018-WEPAF01

A COMPACT PERMANENT MAGNET SPECTROMETER FOR CILEX

M. Khojoyan†, A. Cauchois, J. Prudent, A. Specka
LLR (Laboratoire Leprince-Ringuet), CNRS and Ecole Polytechnique, Palaiseau UMR7638, France

Abstract

Laser Wakefield acceleration experiments make extensive use of small permanent magnets or magnet assemblies for analyzing and focusing electron beams produced in plasma accelerators. Besides being compact, these magnets have to have a large angular acceptance for the divergent laser and electron beams which imposes constraint of the gap size. We will present the optimized design and characterization of a 100 mm long, 2.1 Tesla permanent magnet dipole. Furthermore, we will present the performance of such a magnet as a spectrometer in the CILEX/APOLLON 10 PW laser facility in France.

INTRODUCTION

CILEX (Centre Interdisciplinaire de la Lumiere Extrême / Interdisciplinary Center for Extreme Light) is a research center which aims at using the Apollon-10P laser for exploring laser-matter interaction at extremely high laser intensities (~10^{22} W/cm^2). The long focal length area of CILEX will be used to investigate plasma acceleration and radiation generation. It will be equipped with two interaction chambers able to accommodate laser focal lengths ranging from 3 m to 30 m. The spectrometer magnet presented here is designed to be compatible with the mentioned laser parameters. Sketch of the laser-plasma interaction chamber is shown in Fig. 1. The total volume of interaction chamber is about 3 m^3 and it is practical to use permanent magnets for characterization of electron beam. Permanent magnets, as compared to electromagnets, do not need power supplies (and consequently cooling system) and can be more compact due to smaller apertures. In our case, the apertures of the magnets will be limited by the envelope of the laser, which according to our requirements, should pass through the magnets unobstructed. The paper

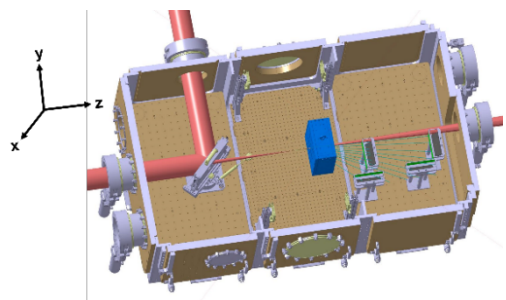

Figure 1: Schematic of interaction chamber at CILEX with laser envelope shown in purple and dipole magnet in blue colors. Measurement screens and reference electron trajectories (green) are shown as well.

is organized as follows. First, the design considerations of a permanent magnetic dipole are introduced together with analytical and computational field estimations. Next, construction of a magnet and field measurements are presented. Finally, the result of beam dynamics simulations implementing 3D magnetic field data are presented by applying the magnet as a spectrometer inside the interaction chamber of the CILEX facility.

† martin.khojoyan@llr.in2p3.fr

MOTIVATION

Let us consider a simple C shaped dipole (Fig. 2). The field in the gap of height h_g is driven by a permanent magnet of the same height $h_{pm} = h_g$ and of width w_{pm}. Assuming constant field in the gap (no horizontal field component) it is straightforward to calculate the magnetic flux density using Ampere's and flux conservation laws:

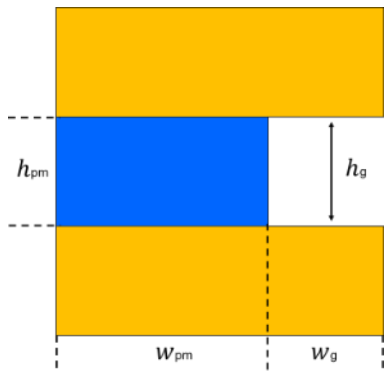

Figure 2: 2D view of a C shaped dipole with a permanent magnet shown in blue and steel/iron in yellow colors.

$$B_g = -\frac{B_r w_{pm}}{w_g + \frac{\mu_r h_g w_{pm}}{h_{pm}}} \quad (1)$$

with B_r and μ_r being the remnant field and relative permeability of the permanent magnet. From Eq. (1) it follows that the maximum achievable field in the gap cannot exceed the remnant induction field of the magnet independent of how small the gap height (h_g) is for reasonably large magnet width (w_g). It becomes clear that for a permanent magnet (PM) dipole, to reach fields higher than remnant field of an individual magnet, a special arrangement of magnetic sub-materials is necessary. Common structures for generating very strong fields are Halbach [1] and Stelter [2] configurations. Nowadays, permanent magnet dipoles are widely used in magnetic resonance imaging applications [3], in facilities such as third [4] and next [5] generation light sources. Neodymium iron Boron (Nd-Fe-B) magnets are the desired candidates for generating strong fields due to their high remnant induction and the highest up to date BH energy product [6]. Moreover, almost linear behaviour of the demagnetization curve [7] and relative permeability close to unity makes the analytical design of such systems relatively straight forward.

ISBN: 978-3-95450-200-4 doi:10.18429/JACoW-ICAP2018-WEPAF01

DESIGN OF A PM DIPOLE

Analytic Estimation of Magnetic Field

For design considerations of a magnetic dipole we assume that the magnet is H shaped with a 2D schematic view (upper half) shown in Fig. 3. The parts shown in yellow color represent iron material: pole tip as well as the yokes for the flux circulation. The pole tip is surrounded by neodymium iron boron magnets with arrows indicating magnetization direction of each magnet. In the same scheme h_g is half the gap height and w / h signify the width / height of each surrounding magnet. The main idea of using such geometry is the collection of the flux from the surrounding permanent magnets and concentration into the magnet gap. The strength of the magnet built in this way can therefore exceed the residual field (B_r) of the permanent magnet materials and, in principle, reach the saturation field of pole material which can be more than 2 Tesla. Next, applying flux conservation and Ampere's laws [8] for the above magnetic circuit (neglecting fringe field effects), one can obtain the following expression for magnetic flux density in the gap:

$$B_g = -\frac{1}{h_g}\frac{\left(w_1 + w_2 + w_3\right)B_r}{\left(\frac{w_g}{h_g} + \frac{\mu_r w_1}{h_1} + \frac{\mu_r w_2}{h_2} + \frac{\mu_r w_3}{h_3}\right)} \qquad (2)$$

It is possible to further optimize the latter expression assuming a square shape magnet poles and similar sizes for surrounding magnets. Since the gain in magnetic field over magnet weight is an important measure in designing the magnet, Fig. 4 illustrates such a dependence for 10 mm gap height. The choice of the gap value is dictated from the magnet exit position compatible with the laser envelope at that position. The indicated field / weight value (red asterisk) on the plot corresponds to a pole size of 51 mm which was chosen according to the commercially available sizes of Nd-Fe-B 40 grade magnets and not from the beam dynamics requirements.

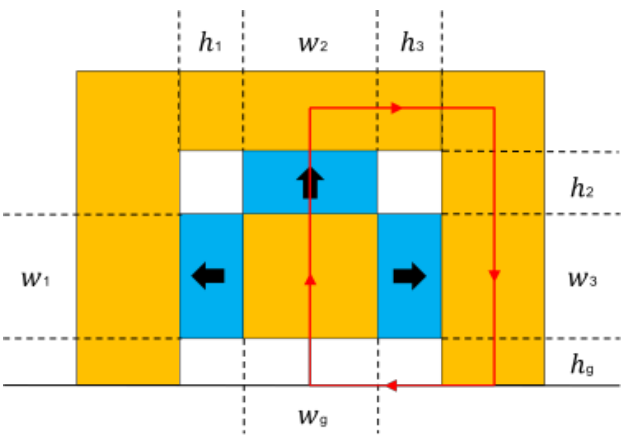

Figure 3: Schematic (2D) view of top half of H shaped magnet with a red flux line following Ampere's law. Iron is shown in yellow with the pole tip surrounded by Neodymium N40 grade magnets expressed in light blue.

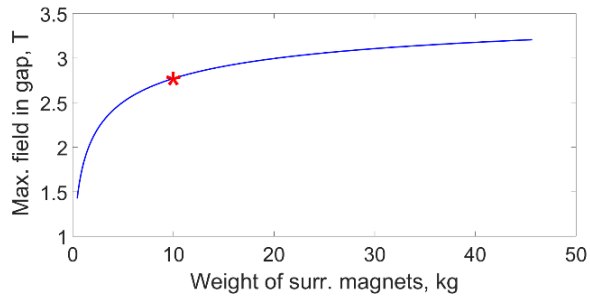

Figure 4: Peak magnetic field vs. total weight of the surrounding magnets shown in Fig. 2. Red asterisk represents the values assuming 51 mm size of each square magnet pole. 10 mm gap size/height is assumed in the plot.

Computation of Magnetic Field

Magnet geometry of Fig. 3 has been studied using three-dimensional TOSCA software [9]. Following dimensions have been used in the calculations: $h_1 = h_3 = 5.08$ cm, $w_1 = w_3 = 7.08$ cm, $h_2 = w_2 = 5.08$ cm. For the case of neodymium magnet, by taking advantage of linear BH behaviour in the second quadrant of BH curve, the slope μ_r can be calculated depending on the grade of the magnet (1.0691 in the case of the Nd-Fe-B 40 grade magnets). Non-linear iron properties have been used in TOSCA for induction versus field data. Due to the symmetry, only one eighth of the magnet geometry was created in 3D TOSCA modeller. A block having a scale factor 3 in all dimensions has been applied as a region of background. The magnetization direction of each magnet was defined by means of Euler angles. 2.5 mm step for meshing yielded over 1.5 million node points for calculation. The aim was to reach magnetic field at the gap as close as possible to the saturation field (2.26 Tesla in this case) of the pole material. A fixed ratio of 20 for magnet gap height over length was imposed. Figure 5 illustrates the expected peak magnetic flux density at the magnet gap for different gap heights obtained from TOSCA simulations (red circles). In the same plot analytical estimation of the field is shown applying an empirical scale factor 2.26 / 2.96, where 2.96 Tesla corresponds to the analytical peak field value for 10 mm gap allowing infinitely high saturation field for the iron. It can be seen from the plot that for the case of 10 mm gap, the value of peak magnetic field in the gap is close to the saturation field of the iron pole and, in the same time, for larger gap sizes the considered geometry is not optimum anymore.

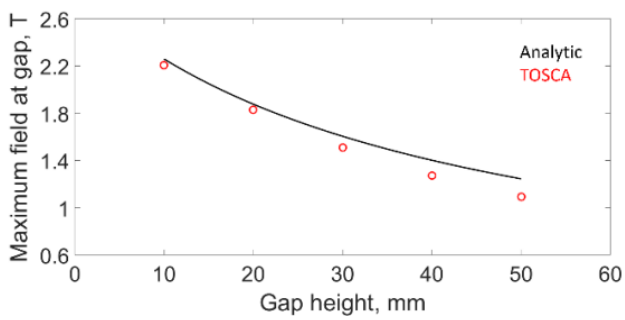

Figure 5: Magnetic induction in the gap for various gap sizes. Red dots: TOSCA calculations. Black curve: analytical estimation applying a factor 0.7635.

ISBN: 978-3-95450-200-4 doi:10.18429/JACoW-ICAP2018-WEPAF01

Construction and Measurements

The PM dipole has been constructed at LLR (Laboratoire Leprince-Ringuet) using Nd-Fe-B 40 grade magnets as surrounding magnet material and allied pure iron (2.18 T saturation field) as pole and yoke material. A dedicated mechanical tooling and careful adjustment were the key points during the magnet assembly due to strong force existent between the magnets and corrosion risks that are not negligible for neodymium magnets. Furthermore, special arrangement of 56 magnets was needed during the assembly to balance the field imperfections of individual magnets (Fig. 6). In Fig. 6, the dimensions ($w \times h \times l$) of the magnets are shown in legends. However, it is believed, that geometry using iron poles will smoothen the effects of field imperfections and defects in magnet once the pole material

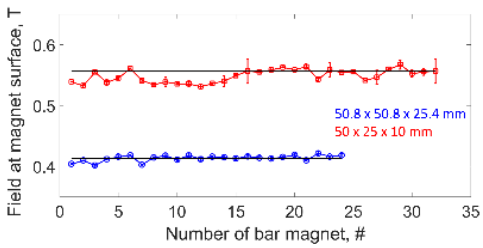

Figure 6: Measured magnetic induction at the surface of two types of neodymium magnets. For each case, black lines represent analytically estimated field values assuming 0.5 mm offset of Hall probe sensor from the magnet surface.

is saturated. The assembled dipole and corresponding TOSCA model of the magnet are presented in Fig. 7. Magnets shown in blue have been added to strengthen the flux on both sides of the poles. The length of the dipole was 100 mm. The assembled magnet was measured at the measurement bench of LLR laboratory. The position of Hall probe was aligned to the magnet using an optical system with high magnification camera (50 µm pixel resolution) in the field of view of 5 cm diameter centered on the pole gap at the magnet exit face (Fig. 8). The Hall probe was mounted on linear translation stages which, according to manufacturer, have 0.07 microradians angular slope and 2 micrometers bidirectional repeatability [10]. Measured and simulated field profiles are plotted in Fig. 9.

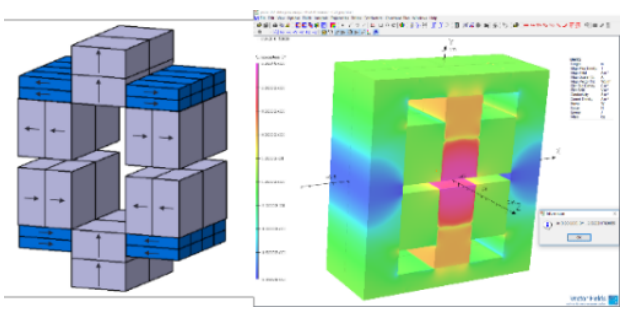

Figure 7: Left: overview of different block magnets used to assembly the dipole. Arrows on the blocks illustrate the magnetization directions. Right: TOSCA model of 100 mm long magnet yielding 2.092 T peak field value in the gap. The main component of induction field is shown in color map from blue (lowest value) to red (highest value).

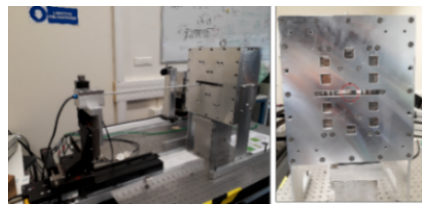

Figure 8: Left: LLR measurement bench with a Hall probe mounted on linear transition stages. Right: defined area of interest for hall probe alignment using optical system.

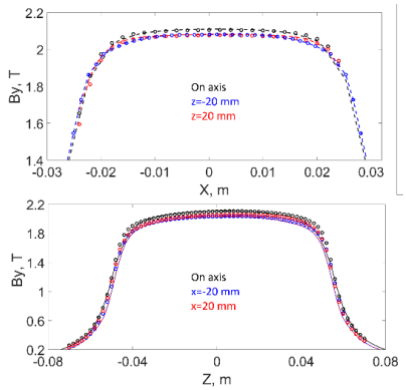

Figure 9: On and off-axis main component field profiles along horizontal (upper plot) and longitudinal (lower plot) directions. For each case dots correspond to the measured and curves to the simulated field values. A scaling factor (~1%) is applied to match the measured and simulated field values.

Table 1: Summary of Magnet Characteristics

Parameter	Value
Gap height, mm	10
Peak field at gap center, T	2.092
Horizontal good field region (~ 10% inhomogeneity), mm	~50
Horizontal full gap region, mm	~150
Length, mm	100
Height, mm	260
Width, mm	240
Weight, kg	~50

The result is remarkable yielding to less than 1% disagreement between predicted and measured field values. The characteristics of the dipole are given in Table 1. No field weakening has been observed as a result of demagnetization effects [11] due to a very strong field at the specific corners of individual magnets (see TOSCA simulation of the magnet on the right side of the Fig. 7).

PM DIPOLE AS A SPECTROMETER

Implementing Magnetic Field Data into ASTRA

ASTRA [12] simulation software has been applied to study the dynamics of different energy electrons through the designed magnet. The magnetic field data has been implemented into ASTRA by means of a Cartesian grid of

ISBN: 978-3-95450-200-4 doi:10.18429/JACoW-ICAP2018-WEPAF01

2 mm × 2 mm × 5 mm ($H \times W \times L$) step size wth corresponding values of field components at each grid point. An idealized electron bunch having Gaussian distribution in all sub spaces was assumed in simulations. Electron beam parameters are summarized in Table 2. The considered energy range of [56–2350] MeV was defined as the lowest energy exiting the magnet from the side of the mechanical gap and the highest energy which is measurable out of 50 milliradians divergent laser cone within the interaction chamber. A 3D space charge routine [13] was applied in ASTRA by using 0.5 million macro particles in a bunch. Electron reference trajectories and various screens (marked as S#) are illustrated in Fig. 10.

Table 2: Electron Beam Parameters used in ASTRA

LPA beam parameter	Value
Charge, pC	10
Peak current, kA	1.2
Energy, MeV	56–2350
Transverse rms size, µm	2.5
Transverse rms divergence, mrad	2

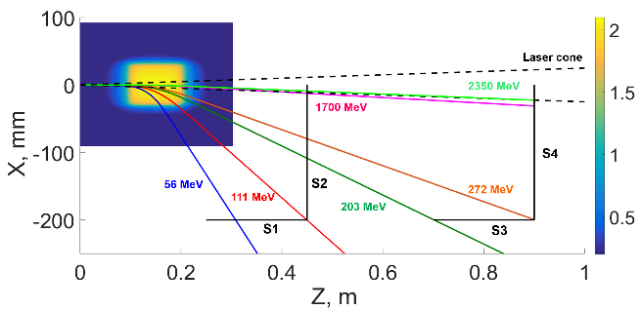

Figure 10: Range of electron trajectories and corresponding screen positions/orientations for energy measurement inside the interaction chamber of CILEX. The laser opening is exemplified by dashed black lines.

Energy Resolution

For each the above-mentioned energy (assuming negligible energy spread) the rms resolution at each screen position was estimated as the ratio of rms beam size in the horizontal plane and the mean beam position. The orientations of the screens have been taken into account in the simulations. Figure 11 plots the beam envelopes at the positions of S1 and S2. In the plot the black line indicates the separation of the screens. Electrons of energies below 200 MeV are strongly affected by the fringe field focusing / defocusing effects. In addition, the fringe field effects may be further enhanced / diminished by adjusting the magnet laterally. The energy resolution at various screens and at different energies is summarized in Fig. 12 yielding less than 8% rms value within the whole energy range for 2 milliradians divergence of electron beam.

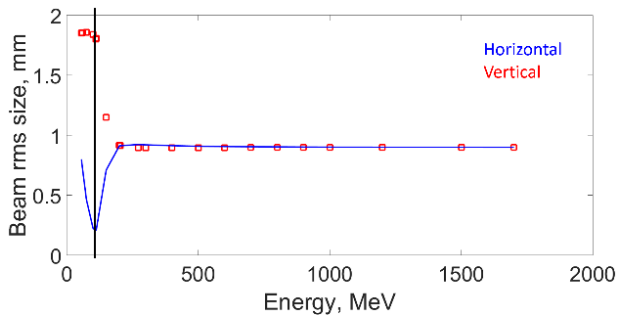

Figure 11: Beam rms transverse sizes at screen positions of S1 and S2. Blue line: horizontal, red rectangles: vertical.

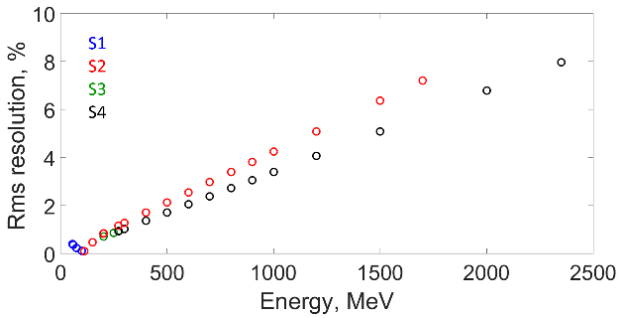

Figure 12: RMS energy resolution estimated at different screens for 2 milliradians beam divergence. Different colors symbolize the outcome at different screen positions.

SUMMARY

A 2.1 Tesla permanent magnet dipole has been designed, constructed, measured and characterized as a spectrometer for CILEX. Very good agreement (~1%) between predicted and measured magnetic field values has been obtained. A precise electron beam tracking has been done afterwards by applying the 3D field map of the magnet into ASTRA simulation program. According to tracking results the magnet will enable to measure electrons from 56 MeV to 2.35 GeV with rms resolution of below 8 percent at full energy range. Besides, for smaller laser divergence the magnet can be shifted downstream and the energy resolution may be improved by adding a focusing element into the configuration.

ACKNOWLEDGMENTS

The work is partially supported by the European Union's Horizon 2020 Research and innovation program under grant agreement No 730871.

REFERENCES

[1] K. Halbach, "Application of permanent magnets in accelerators and electron storage rings", *Journal of Applied Physics,* vol. 57, pp. 3605, 1985.

[2] R. E. Stelter, "Dipole permanent magnet structure", United States patent, 1997.

[3] K. Halbach, "Design of permanent multipole magnets with oriented rare earth cobalt material", *Nuclear Instruments and Methods*, vol. 169, 1980.

ISBN: 978-3-95450-200-4 doi:10.18429/JACoW-ICAP2018-WEPAF01

[4] C. Li, "Efficiency of permanent magnet assemblies for MRI devices", *IEEE Transactions on Magnetics*, vol. 41, pp. 10, 2005.

[5] G. Tosin *et al.*, "Bending magnets made with permanent magnets for LNLS-2 electron storage ring", in *Proc. PAC'09,* Vancouver, Canada, May 2009, paper MO6PFP001.

[6] S.C. Gottschalk *et al.*, "Permanent magnet systems for free-electron lasers", *Nuclear Instruments and Methods in Physics Research* A, vol. 507, pp. 181-185, 2003.

[7] J. F. Herbst *et al.*, "Structural and magnetic properties of Nd2Fe14B", *J. Appl. Phys*., vol. 57, pp. 4086, 1985.

[8] B. C. Brown, "Design formulas for the strength, compensation and trimming of hybrid permanent magnets", FERMILAB-Conf-96/273, 1996.

[9] TOSCA, Opera-3d, Cobham Technical Services, Software for electromagnetic design, Oxford, UK http://operafea.com/

[10] Thorlabs: Linear Translation Stages, https://www.thorlabs.com/newgrouppage9.cfm?objectgroup_id=7652

[11] M. Katter, "Angular dependence of the demagnetization stability of sintered Nd-Fe-B magnets", *IEEE Transections on Magnetics*, vol. 41, pp. 10, 2005.

[12] K. Floettmann, ASTRA, http:/www.desy.de/mpyflo

[13] G. Poplau *et al.*, "3D space charge calculations for bunches in the tracking code ASTRA", in *Proc. EPAC'06*, Edinburgh, UK, Jun 2006, paper WEPC121.